

An enzyme-coupled biosensor enables (S)-reticuline production in yeast from glucose

William C DeLoache¹, Zachary N Russ¹, Lauren Narcross^{2,3}, Andrew M Gonzales¹, Vincent J J Martin^{2,3} & John E Dueber^{1*}

Benzyloquinoline alkaloids (BIAs) are a diverse family of plant-specialized metabolites that include the pharmaceuticals codeine and morphine and their derivatives. Microbial synthesis of BIAs holds promise as an alternative to traditional crop-based manufacturing. Here we demonstrate the production of the key BIA intermediate (S)-reticuline from glucose in *Saccharomyces cerevisiae*. To aid in this effort, we developed an enzyme-coupled biosensor for the upstream intermediate L-3,4-dihydroxyphenylalanine (L-DOPA). Using this sensor, we identified an active tyrosine hydroxylase and improved its L-DOPA yields by 2.8-fold via PCR mutagenesis. Coexpression of DOPA decarboxylase enabled what is to our knowledge the first demonstration of dopamine production from glucose in yeast, with a 7.4-fold improvement in titer obtained for our best mutant enzyme. We extended this pathway to fully reconstitute the seven-enzyme pathway from L-tyrosine to (S)-reticuline. Future work to improve titers and connect these steps with downstream pathway branches, already demonstrated in *S. cerevisiae*, will enable low-cost production of many high-value BIAs.

Plant-specialized metabolites are a rich source of chemical diversity that has given rise to a host of prominent pharmaceuticals¹. Despite their widespread use², many of these compounds are still manufactured from plant extracts because they are too structurally complex to be cost-effectively produced by total organic synthesis. Target metabolites often accumulate at low levels in plants, and efforts to improve yields are hindered by limitations in plant metabolic engineering, namely complex pathway regulation, a lack of genetic tools and long development cycles³. Such problems have also made it challenging to fully explore the potential structural diversity of natural product derivatives⁴.

Microbially based production systems overcome many of these barriers and are poised to transform the manufacturing and drug discovery processes for many natural products⁵. Next-generation DNA sequencing has accelerated the elucidation of complex biochemical pathways in plants such that they can now be transplanted to easily engineered and scalable industrial production hosts⁶. Meanwhile, the development of powerful synthetic biology tools for genetically manipulating cells has made the engineering of microorganisms with new properties considerably faster, cheaper and easier^{7,8}. Commercial production of the antimalarial drug precursor artemisinic acid in the yeast *S. cerevisiae* is a pioneering example of these technologies revolutionizing pharmaceutical manufacturing⁹.

BIAs are a large family of L-tyrosine-derived plant-specialized metabolites with a variety of therapeutic uses¹⁰. This class of compounds includes the opioid analgesics morphine and codeine, the antibiotics sanguinarine and berberine, the muscle relaxants (+)-tubocurarine and papaverine and the cough suppressant noscapine. Several analgesics (for example, oxycodone) are synthetic derivatives of the BIA intermediate thebaine¹⁰. Because of their structural complexity, most BIAs cannot be chemically synthesized at commercial scale and are instead extracted from plants, most notably the opium poppy (*Papaver somniferum*)¹¹. In light of recent advances in our understanding of BIA biosynthesis, these molecules have become high-value targets for production via microbial fermentation.

A major achievement in microbial BIA production was marked by the synthesis of the key intermediate (S)-reticuline from glucose in the bacterium *Escherichia coli*¹². (S)-Reticuline is the final intermediate to be shared between the major branches of the BIA pathway. Despite high titers¹³, no steps downstream of (S)-reticuline have since been demonstrated in *E. coli*. However, an impressive number of these downstream steps have been successfully reconstituted in *S. cerevisiae*, leading to the recent production of many valuable BIAs, albeit from cost-prohibitive intermediates such as norlaudanoline and thebaine^{14–16}. These products include morphine, codeine, hydrocodone, hydromorphone, oxycodone, (S)-tetrahydroberberine and dihydrosanguinarine. *S. cerevisiae* is amenable to the functional expression of endomembrane-localized cytochrome P450s and therefore is a more suitable host for the downstream steps of BIA biosynthesis⁸. P450s have an important role in BIA synthesis and diversification, especially in the generation of new backbones such as morphinans (CYP719B1), aporphines (CYP80G2), bisbenzyloquinolines (CYP80B2) and benzophenanthridines (CYP82N4)¹⁰. Although yeast have been cocultured with reticuline-producing *E. coli* to catalyze downstream steps to magnoflorine and scoulerine¹⁷, large-scale production of BIAs will most likely necessitate that all steps be consolidated into a single microorganism to minimize carbon loss and simplify fermentation processes. Although there have been recent successes in establishing microbial cocultures and sequential fermentations in the laboratory^{13,18,19}, industrial fermentations frequently favor monocultures over more complicated, multistrain strategies.

Production of (S)-reticuline from central metabolites in *S. cerevisiae* has proven unexpectedly difficult given the early successes in *E. coli*. Although reticuline has been synthesized from fed norlaudanoline in yeast¹⁴, the upstream steps required for the synthesis of norlaudanoline or the natural BIA backbone (S)-norcoclaurine from L-tyrosine have remained elusive. This is primarily attributable to difficulties at the first biosynthetic step from L-tyrosine to L-DOPA as well as poor activity of the norcoclaurine synthase (NCS)²⁰. Prior to this work, there were two known families

¹Department of Bioengineering, University of California, Berkeley, Berkeley, California, USA. ²Department of Biology, Concordia University, Montréal, Québec, Canada. ³Centre for Structural and Functional Genomics, Concordia University, Montréal, Québec, Canada. *e-mail: jdueber@berkeley.edu

of enzymes broadly referred to as tyrosine hydroxylases. Plants and animals use tyrosine 3-monooxygenases (EC 1.14.16.2), which require a cofactor (tetrahydrobiopterin) not found in yeast²¹. Copper-containing tyrosinases (EC 1.14.18.1), used by many organisms for melanin production, exhibit both tyrosine hydroxylase and DOPA oxidase activities to produce L-dopaquinone from L-tyrosine^{22,23}. Although bacterial tyrosinases have been used for L-DOPA production in *E. coli*¹², functional expression of these enzymes in *S. cerevisiae* remains a challenge.

To aid in the search for a yeast-active tyrosine hydroxylase, we developed an enzyme-coupled biosensor for the BIA pathway intermediate L-DOPA. This biosensor takes advantage of a plant biosynthetic enzyme that converts L-DOPA into the yellow, fluorescent pigment betaxanthin²⁴. Using this sensor, we identified a tyrosine hydroxylase that was highly active in *S. cerevisiae* and were able to further improve its activity via PCR mutagenesis to increase L-DOPA titer by 2.8-fold and dopamine titer by 7.4-fold. This enzyme is a cytochrome P450 from the sugar beet *Beta vulgaris* and represents what is to our knowledge the first known example of a P450 capable of L-tyrosine hydroxylation. Although the wild-type version of this enzyme catalyzes an additional unwanted oxidation of L-DOPA into L-dopaquinone, one of the beneficial mutations that we identified suppresses this off-pathway activity. Our mutant tyrosine hydroxylase enabled the production of dopamine in yeast and, when coupled to a newly identified NCS from opium poppy, allowed for the synthesis of the BIA intermediates (S)-norcoclaurine and (S)-reticuline from glucose. By connecting the central metabolism of yeast to the downstream steps of BIA biosynthesis that have previously been demonstrated in *S. cerevisiae*, this work accelerates the development of a microorganism capable of producing high-value BIAs at commercial scale.

RESULTS

Development of an enzyme-coupled L-DOPA biosensor

A long-standing inability to achieve L-tyrosine hydroxylation to L-DOPA in yeast prompted us to develop an enzyme-coupled biosensor for L-DOPA that could be used to quickly screen candidate tyrosine hydroxylases for activity. DOPA dioxygenase (DOD) is a plant enzyme found in members of the order Caryophyllales that converts L-DOPA into a yellow, highly fluorescent family of pigments called betaxanthins (Fig. 1a)^{25,26}. These betaxanthins, all of which have similar optical properties, are the result of a spontaneous reaction between free amines and betalamic acid produced by DOD (Supplementary Results and Supplementary Fig. 1)²⁷. For simplicity, we will refer to this entire family of molecules collectively as betaxanthin.

We expressed in yeast a DOD variant from the flowering plant *Mirabilis jalapa*²⁵ and found that cells grown in medium supplemented with L-DOPA produced enough betaxanthin to be easily detected by eye in both the supernatant and the cell pellet. Fluorescence microscopy indicated that betaxanthin, which is highly water soluble, accumulates in the yeast vacuole in addition to getting pumped out of the cell through unknown mechanisms (Fig. 1b). Because a substantial fraction of betaxanthin remains intracellular, L-DOPA levels can be quantified via cellular fluorescence. Using a microplate fluorometer, we generated a dose-response curve for a DOD-expressing strain grown in 0.1–10,000 μM L-DOPA (Fig. 1c). Changes in betaxanthin fluorescence were detectable across a range of three orders of magnitude from 2.5 μM to 2,500 μM L-DOPA, with the most sensitive response observed between 25 μM and 250 μM L-DOPA (Supplementary Fig. 2). The sensor demonstrated a 110-fold dynamic range and low sample-to-sample variability, yielding a Z'-factor of 0.91, where a value between 0.5–1.0 typically denotes an excellent high-throughput assay²⁸. Changes in betaxanthin fluorescence were also readily detectable at the single-cell level via flow cytometry (Fig. 1d). Using this detection technique, we achieved

a 145-fold dynamic range for the sensor; however, we observed considerable cell-to-cell variability, as is common for single-cell measurements, despite both gating cells by forward and side scatter and normalizing fluorescence by forward scatter to account for differences in cell size (Supplementary Figs. 3 and 4). Analysis of our flow cytometry data indicated that a tyrosine hydroxylase variant with twofold improved activity would be expected to be enriched between 25- and 50-fold over the rest of the population in a given round of fluorescence-activated cell sorting (FACS) if L-DOPA production fell in the linear range of the biosensor. Although the ability to cell sort is promising for enabling future screens and applications, we elected to use colony-based colorimetric and fluorometric screening of our tyrosine hydroxylase libraries, as this technique proved sufficient for our purposes (Supplementary Fig. 5).

Notably, our enzyme-coupled biosensor is designed to be specific for L-DOPA as it should be capable of differentiating between the tyrosine hydroxylase and DOPA oxidase activities exhibited by tyrosinases. For the production of BIAs, the secondary DOPA oxidase activity is undesirable as it diverts L-DOPA to melanin²⁹. Although a tyrosinase from the button mushroom *Agaricus bisporus* (polyphenol oxidase 2 (AbPPO2)) has been successfully expressed in yeast, this enzyme had over tenfold higher activity on L-DOPA than it did on L-tyrosine³⁰. Given the existence of bacterial tyrosinases with relatively low DOPA oxidase activity³¹, we hypothesized that our betaxanthin production assay could be used alongside enzyme mutagenesis to alter the relative substrate specificity for L-DOPA and L-tyrosine in enzymes that preferentially act on L-DOPA and are active in yeast. In this manner, undesired DOPA oxidase activity (activity 2; Fig. 1a and Supplementary Fig. 1) could be minimized and tyrosine hydroxylase activity maximized (activity 1; Fig. 1a and Supplementary Fig. 1).

Identification of a yeast-active tyrosine hydroxylase

We first sought a tyrosine hydroxylase variant that yielded measurable levels of betaxanthin when expressed with DOD to use as a starting point for enzyme mutagenesis. Although we expected this search to involve screening large variant libraries from cDNA or bioinformatic curation, we fortuitously found an acceptable candidate without resorting to these techniques. We note that future work to screen such libraries with our enzyme-coupled biosensor might reveal additional insights into this enzyme class and even identify variants with higher activity than those described in this work. Two candidate enzymes were selected for initial screening: AbPPO2 from *A. bisporus* (discussed above) and CYP76AD1 from the sugar beet *B. vulgaris*. The latter is a recently identified cytochrome P450 DOPA oxidase³². This enzyme is responsible for the production of the violet pigment betanidin (a betaxanthin analog) in beets (Supplementary Fig. 1). Functional expression of CYP76AD1 in yeast was previously demonstrated to elucidate this enzyme's role in determining beet color, making it an attractive candidate for our purposes³². Notably, tyrosine hydroxylase activity was not previously reported for this enzyme; it was selected with the objective of altering its substrate specificity from L-DOPA to L-tyrosine.

Both AbPPO2 and CYP76AD1 were codon optimized for yeast and expressed along with DOD. As expected from previous work, AbPPO2 showed extremely low, but detectable, betaxanthin production. To our surprise, CYP76AD1 exhibited considerable tyrosine hydroxylase activity, leading to levels of betaxanthin that were clearly visible in colonies growing on agar plates (Fig. 2a). This result was particularly unexpected given previous work in which CYP76AD1 and a DOD were coexpressed in yeast and yielded no observable betaxanthin³². One experimental difference that could account for these contradictory results is the identity of the DOD enzyme used. While our strains used a DOD from *M. jalapa*, previous experiments with CYP76AD1 were conducted using a *B. vulgaris* DOD, which has a K_m of 7 mM³³, well above the levels

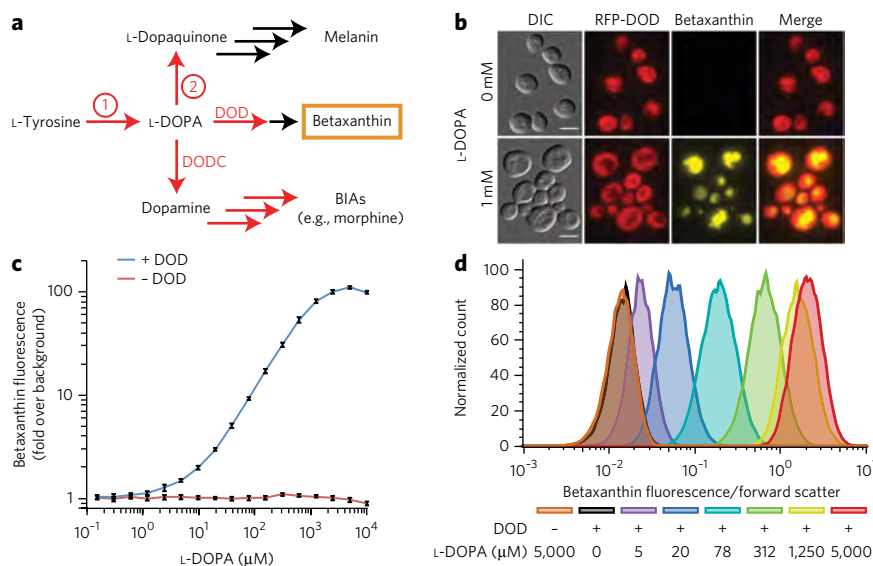


Figure 1 | Development and characterization of an enzyme-coupled L-DOPA biosensor.

(a) L-DOPA can be acted on by three distinct enzymes. For the production of BIAs, DODC is the desired activity. However, many enzymes that produce L-DOPA (tyrosine hydroxylases, activity 1) also have a second activity (DOPA oxidase, activity 2) that introduces a competing pathway to melanin. DOD converts L-DOPA into the fluorescent, yellow pigment betaxanthin in plants and was used in yeast as an L-DOPA biosensor to optimize tyrosine hydroxylase activity. Red arrows denote enzymatic reactions; black arrows denote spontaneous reactions. See **Supplementary Figure 1** for a more detailed pathway diagram. (b) Fluorescence microscopy of yeast cells expressing DOD with the red fluorescent protein (RFP) mKate2 fused to the N terminus, grown in medium with and without L-DOPA . Scale bars, 10 μm . (c) Dose-response curve for a DOD-expressing strain (blue) and a wild-type control strain (red) grown in medium supplemented with a range of L-DOPA concentrations ranging from 10,000 μM to 0.15 μM in twofold increments. Cellular betaxanthin fluorescence was measured on a microplate fluorometer. Error bars represent mean \pm s.d. of twelve biological replicates. (d) Flow cytometry histograms for DOD-expressing yeast cells (and a wild-type control, orange) grown in medium supplemented with a range of L-DOPA concentrations. Cells were gated by forward and side scatter as indicated in **Supplementary Figure 3**. Betaxanthin fluorescence was normalized to forward scatter to account for variation in cell size. Cell counts were normalized as a percent of the mode of each population.

that are likely to accumulate in yeast given the competing DOPA oxidase activity of CYP76AD1.

After achieving clearly detectable betaxanthin synthesis with CYP76AD1, we tested for L-DOPA production in the absence of DOD. CYP76AD1 yielded 1.3 mg l^{-1} L-DOPA , almost 20 times the levels obtained with AbPPO2. This result suggested that our betaxanthin biosensor would have utility in further optimizing L-DOPA production, as the betaxanthin levels from AbPPO2 and CYP76AD1 were predictive of L-DOPA titers (**Fig. 2b**). We hypothesized that titers could be improved by abolishing CYP76AD1's DOPA oxidase activity and set out to perform mutagenesis and screening with our L-DOPA biosensor.

Improving tyrosine hydroxylase activity

We performed error-prone PCR to generate a library of CYP76AD1 mutants that was transformed into a yeast strain expressing DOD. This mutant library contained approximately 200,000 members with an average mutation rate of approximately four mutations per gene. The difference in betaxanthin production between library clones was sufficiently large that obvious differences between colonies could be detected by eye with the aid of blue light epi-illumination and an amber-green emission filter to amplify the betaxanthin fluorescence signal (**Supplementary Fig. 5**). We visually selected 17 of the highest betaxanthin producers for sequence analysis and

confirmation of activity using microplate fluorometry (data not shown). Six of the seventeen clones that we sequenced contained the same F309L missense mutation; among those with this mutation, there were two distinct genotypes.

We narrowed our set of hits to six by removing duplicate genotypes and any mutant proteins that showed less than a 1.5-fold improvement in betaxanthin production upon isolation and retransformation into the L-DOPA sensor base strain (**Supplementary Fig. 6**). These six mutants were used to construct a DNA shuffling library to randomly combine potentially beneficial mutations. The resulting library was again transformed into yeast expressing DOD and screened for betaxanthin production through a combination of visual screening and plate-based fluorescence measurements. We visually selected 67 high-fluorescence colonies to grow in liquid medium, and secondary fluorescence screening was done in a microplate format (**Supplementary Fig. 7**). Out of the 28 highest producers that we sequenced from the DNA shuffling library, 20 had incorporated the same two mutations (W13L and F309L), suggesting that the effects of these mutations were multiplicative. An additional silent mutation that was linked to W13L (9T>C) was also enriched for and included in future experiments involving the W13L mutation. This linked double mutation will be referred to as W13L for convenience.

Because W13L and F309L seemed to be our two best mutations, we analyzed their effects on betaxanthin and L-DOPA production individually and in combination. Compared to wild-type CYP76AD1, the W13L and F309L single mutants yielded 1.7-fold and 1.9-fold more betaxanthin, respectively (Z-scores of 16.2 and 21.0, respectively) when measured on a microplate fluorometer (**Fig. 2b**). When combined, the double mutant showed a net increase in betaxanthin fluorescence of 2.7-fold over wild-type CYP76AD1 with a Z-score of 10.0 relative to the F309L single mutant. When betaxanthin fluorescence was compared via flow cytometry, the mutant populations were easily distinguishable, showing a 4.3-fold improvement in mean fluorescence for the double mutant compared to wild-type CYP76AD1 (**Supplementary Fig. 8**). In the absence of DOD, CYP76AD1 with the W13L, F309L and W13L F309L mutations improved upon the L-DOPA titer of wild-type CYP76AD1 by 1.9-fold, 1.4-fold and 2.8-fold, respectively (**Fig. 2b**). Overall, there was a strong linear correlation between betaxanthin fluorescence and intracellularly produced L-DOPA ($R^2 = 0.92$), although there was a slight discrepancy between the two measurements for the F309L mutant.

We next tested the ability of CYP76AD1 to catalyze the synthesis of the downstream BIA intermediate dopamine when expressed with a DOPA decarboxylase (DODC) from *Pseudomonas putida* that is highly specific for L-DOPA ³⁴. The specificity of DODC is important, as decarboxylation of L-tyrosine would introduce a side pathway to tyramine and reduce flux to dopamine¹². When combined into a single strain, both activities resulted in dopamine production, something that to our knowledge has not been demonstrated previously in *S. cerevisiae*. Using wild-type CYP76AD1, we achieved a dopamine titer of 1.5 mg l^{-1} (**Fig. 2c**). Both the W13L and F309L single

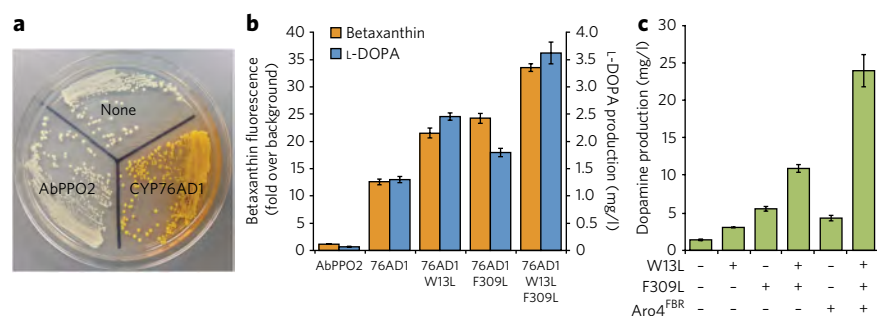


Figure 2 | Isolation and improvement of a tyrosine hydroxylase in yeast. (a) Yeast cells expressing DOD alone or with a candidate tyrosine hydroxylase (either AbPPO2 from *A. bisporus* or CYP76AD1 from *B. vulgaris*), streaked on an agar plate with synthetic complete medium. **(b)** Quantification of tyrosine hydroxylase activity for enzyme variants isolated with the betaxanthin biosensor screen. Yellow bars represent betaxanthin fluorescence in cells coexpressing a tyrosine hydroxylase variant with DOD as measured by cellular fluorescence on a microplate fluorometer. Fluorescence values were normalized to the autofluorescence of a control strain that expressed no tyrosine hydroxylase. Blue bars show L-DOPA titer after 48 h of growth for strains expressing a candidate tyrosine hydroxylase as measured by LC/MS of culture supernatants and comparison to a standard curve. Amino acid substitutions are listed for enzyme mutants (76AD1 represents CYP76AD1). Error bars indicate mean \pm s.d. of four biological replicates. **(c)** Dopamine titers in the culture supernatant of cells coexpressing DOD and a CYP76AD1 mutant as measured by LC/MS and comparison to a standard curve. The presence of the W13L and/or F309L mutation in a given variant is indicated with a +. A strain overexpressing a feedback resistant mutant of Aro4p, known to increase intracellular tyrosine levels (Aro4^{FBR}), was also tested with select CYP76AD1 variants. Error bars indicate mean \pm s.d. of four biological replicates.

mutants improved dopamine production; in fact, the effect of the F309L mutant on dopamine titer was considerably larger than had been observed for L-DOPA titer (3.8-fold versus 1.4-fold, respectively). The W13L F309L double mutant of CYP76AD1 increased the level of dopamine production to an unexpectedly high 10.8 mg l⁻¹, a level 7.4-fold greater than that in the wild-type enzyme.

Given the high tyrosine hydroxylase activity of the CYP76AD1^{W13L F309L} double mutant, we hypothesized that L-tyrosine availability might be limiting dopamine production in our strain. Therefore, we overexpressed a feedback-insensitive mutant of the L-tyrosine pathway enzyme Aro4p that is known to markedly increase the intracellular L-tyrosine concentration in *S. cerevisiae*³⁵. Doing so resulted in an additional 2.2-fold increase in dopamine levels. In this strain background, we achieved a final dopamine titer of 23.8 mg l⁻¹ when cells were grown for 48 h in 2 \times synthetic complete medium with 4% glucose (Fig. 2c).

Characterization of reduced DOPA oxidase activity

We were interested in characterizing the mechanism by which our CYP76AD1 mutants led to increased tyrosine hydroxylase activity and started by looking at changes in enzyme expression. Western blot analysis showed that the W13L mutation yielded 2.8-fold more protein, whereas the F309L mutation led to a 1.6-fold increase in expression (Fig. 3a and Supplementary Fig. 9). These changes were consistent with measurements of protein expression made via fluorescent protein fusion (Supplementary Fig. 10). Fluorescence microscopy of these fusion proteins showed that neither mutation affected localization of CYP76AD1 to the endoplasmic reticulum (Supplementary Fig. 11). Although increased expression is sufficient to explain the improvements in L-DOPA and dopamine production caused by the W13L mutation, the 3.8-fold improvement in dopamine titer caused by the F309L mutation cannot be fully explained by a 1.6-fold increase in protein abundance. Therefore, we investigated potential changes in catalytic activity resulting from this mutation.

While pelleting L-DOPA-producing cultures overexpressing feedback-insensitive Aro4p, we noticed that cells expressing wild-type CYP76AD1 or the W13L single mutant were brown in color compared to cells expressing a version of CYP76AD1 incorporating the F309L mutation (Fig. 3b). We suspected that this brown color was most likely due to the accumulation of melanin generated by CYP76AD1's DOPA oxidase activity (Fig. 3c). Because of challenges associated with accurate quantification of melanin and its precursor, L-dopaquinone (Supplementary Fig. 12), we again turned to the betaxanthin pathway to analyze this apparent change in CYP76AD1's catalytic activity. As stated previously, the pathway from L-DOPA to betaxanthin goes through the intermediate betalamic acid, which undergoes spontaneous condensation with amines (Supplementary Fig. 1). If L-dopaquinone is generated via a DOPA oxidase, however, betalamic acid can react with the L-dopaquinone derivative cyclo-DOPA to form a violet pigment called betanidin (Fig. 3c and Supplementary Fig. 1).

We used betanidin production as an indicator of DOPA oxidase activity in yeast. Doing so required supplementing the growth medium with ascorbic acid as a reducing agent to prevent spontaneous betanidin oxidation, which causes the pigment to polymerize and lose its violet color³⁶.

When coexpressed with DOD, candidate tyrosine hydroxylases with high DOPA oxidase activity should produce a violet supernatant containing high levels of betanidin, whereas enzymes with low DOPA oxidase activity will generate a yellow supernatant that is composed mostly of betaxanthin and betalamic acid. As expected, when wild-type CYP76AD1 was tested in this betaxanthin-betanidin assay, the supernatant was violet, indicating high DOPA oxidase activity (Fig. 3d). Although the W13L mutation increased the concentration of pigments in the culture supernatant, the overall violet color did not change (Supplementary Fig. 13). In contrast, incorporation of the F309L point mutation into CYP76AD1 produced a shift in color from violet to yellow, which was also observed for the W13L F309L double mutant. This change demonstrates that the F309L mutation reduces DOPA oxidase activity. To better quantify the culture supernatants, we measured betanidin and betaxanthin using LC/MS. Tyrosine-betaxanthin was selected as a representative member of the betaxanthin species as many different betaxanthins can form from the spontaneous condensation of an amine with betalamic acid (Supplementary Fig. 14). Our results showed that betanidin levels decreased by 80% in the F309L mutant, compared to wild-type CYP76AD1 (Fig. 3e). This decrease in betanidin was accompanied by a 3.7-fold increase in tyrosine-betaxanthin production. When quantified via LC/MS, the changes in tyrosine-betaxanthin caused by the mutations showed a strong linear correlation to the dopamine levels measured in Figure 2c ($R^2 = 0.999$; Supplementary Fig. 15). In fact, betaxanthin titers were more predictive of dopamine titers than direct measurement of L-DOPA in the absence of a downstream enzyme.

To further investigate the importance of the F309 residue on DOPA oxidase activity, we performed a protein alignment of CYP76AD1 to its three known orthologs (CYP76AD2, CYP76AD3 and CYP76AD4), which showed that this residue is conserved in each (Supplementary Fig. 16). To determine whether the F309L mutation would have similar effects in these orthologs, we

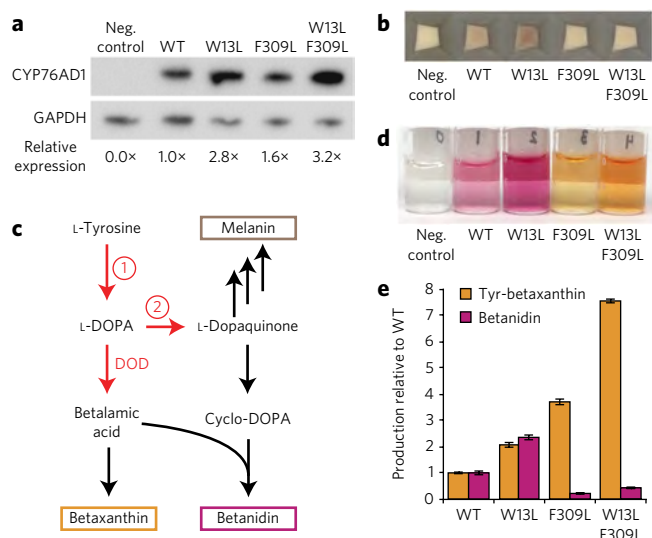


Figure 3 | Characterization of reduced DOPA oxidase activity in

CYP76AD1 mutants. (a) Western blot comparing expression level of CYP76AD1 mutants in yeast. Enzymes contain a C-terminal Flag tag. An anti-GAPDH antibody was used as a loading control. Relative expression represents the ratio of anti-Flag intensity to anti-GAPDH intensity, normalized to wild-type (WT) CYP76AD1. (b) Pelleted yeast cells expressing CYP76AD1 mutants (and Aro4^{FR}). The negative (Neg) control denotes a strain not expressing CYP76AD1. (c) DOD generates the intermediate betalamic acid that can either react with free amines to produce betaxanthins (a yellow family of pigments) or with the L-dopaquinone derivative cyclo-DOPA to produce betanidin (a violet pigment). Betanidin is labile but can be stabilized with the addition of the reducing agent ascorbic acid. Relative levels of betanidin production were used to compare DOPA oxidase activity (activity 2) in CYP76AD1 variants. See **Supplementary Figure 1** for a more detailed pathway diagram. (d) Culture supernatant from strains coexpressing DOD and a CYP76AD1 mutant grown in minimal medium with ascorbic acid. Negative control indicates no CYP76AD1 expression. (e) LC/MS analysis of tyrosine-betaxanthin (yellow) and betanidin (violet) levels in the supernatants from **d**. Tyrosine-betaxanthin was selected as a representative member of the betaxanthins as many different species exist in the culture supernatant. Peak areas were fit to relative standard curves generated by serial dilution of the samples to obtain levels of betanidin and tyrosine-betaxanthin relative to the wild-type CYP76AD1 sample. Error bars represent mean \pm s.d. of four biological replicates.

codon-optimized the genes for expression in yeast and tested wild-type and F309L mutants in the betaxanthin-betanidin assay. In all of the cases, introduction of the mutation produced a shift from violet to yellow supernatants (**Supplementary Fig. 17**). We further aligned the CYP76AD1 protein sequence to its seven closest paralogs from the recently sequenced beet genome and found that all seven contained the same F309L substitution that we had identified through PCR mutagenesis (**Supplementary Fig. 18**)³⁷. In beets, inactivation of CYP76AD1 abolishes betanidin production, whereas betaxanthin production persists, suggesting the presence of a dedicated tyrosine hydroxylase for betanidin synthesis³². We tested the two closest paralogs for tyrosine hydroxylase activity in *S. cerevisiae* but observed no betaxanthin production (data not shown). Efforts to determine a crystal structure for CYP76AD1 were unsuccessful, but a homology model was generated by threading CYP76AD1 onto human CYP1A2 (**Supplementary Fig. 19**)³⁸. The model provided little insight into the mechanism of the F309L mutation's effect on CYP76AD1's behavior as the residue was 14 Å from the enzyme's predicted active site.

Production of (S)-reticuline from glucose

Having achieved efficient dopamine production from L-tyrosine in *S. cerevisiae*, we sought to extend the pathway toward downstream BIA intermediates. The first committed step in BIA biosynthesis is the formation of the backbone molecule (S)-norcoclaurine via condensation of dopamine and 4-hydroxyphenylacetaldehyde (4-HPAA), a reaction that is catalyzed by NCS (**Fig. 4a**). 4-HPAA is produced endogenously in *S. cerevisiae* as an intermediate of the Ehrlich pathway for amino acid catabolism³⁹. In this pathway, L-tyrosine is converted to 4-HPAA through sequential transamination and decarboxylation reactions before being broken down into tyrosol or 4-hydroxyphenylacetate (4-HPA) by a host of redundant enzymes.

From (S)-norcoclaurine, four additional enzymatic steps are needed to produce (S)-reticuline, the last shared intermediate of the major BIA pathway branches (**Supplementary Fig. 20**). Three of these enzymes catalyze methylation reactions: 6-O-methyltransferase (6OMT), coclaurine N-methyltransferase (CNMT) and 4'-O-methyltransferase (4'OMT). Variants of each methyltransferase from *P. somniferum* have been demonstrated to function in *S. cerevisiae*¹⁴. The remaining enzyme is the cytochrome P450 N-methylcoclaurine hydroxylase (NMCH; also known as CYP80B1). Previous work to synthesize reticuline in *S. cerevisiae* circumvented this enzyme by feeding a hydroxylated derivative of norcoclaurine, norlaudanosoline, which is commercially available, albeit expensive. NMCH has, however, been isolated from the California poppy (*Eschscholzia californica*) and successfully expressed and purified heterologously from *Spodoptera frugiperda* Sf9 cells⁴⁰.

We divided the (S)-reticuline pathway into three modules (**Fig. 4a**). Module A combines our best tyrosine hydroxylase mutant (CYP76AD1^{W13L F309L}) and DODC to produce dopamine. We relied on endogenous yeast enzymes for 4-HPAA production, although our strains did overexpress feedback-insensitive Aro4p, which increases flux through 4-HPAA in addition to increasing L-tyrosine levels. Module B included an NCS from *P. somniferum* (GenBank accession code [KP262411](#)), which was selected after screening four NCS variants with homology to a *Thalictrum flavum* NCS (GenBank accession code [ACO90248.1](#)) for activity in *S. cerevisiae* (**Supplementary Fig. 21**)⁴¹. Module C consists of the four enzymes required for the conversion of (S)-norcoclaurine to (S)-reticuline, including 6OMT, CNMT and 4'OMT from *P. somniferum* and NMCH from *E. californica*. We constructed three strains for testing, which we refer to here by the pathway modules that they express (A, AB and ABC). All heterologous genes in these strains are expressed using high-strength promoters and are either integrated into the chromosome (modules A and B) or maintained on a low-copy plasmid (module C).

Strain AB produced easily detectable levels of norcoclaurine when grown in synthetic complete medium with glucose (**Fig. 4b,c**). Given that this product was not observed in the supernatant of strain A, norcoclaurine synthesis (which can occur spontaneously in other systems¹³) seemed to be dependent on NCS expression. Although spontaneously formed norcoclaurine is racemic, NCS is known to be stereoselective, producing only (S)-norcoclaurine⁴². Chiral analysis confirmed that all of the norcoclaurine produced by strain AB was the (S)-enantiomer (**Supplementary Fig. 22a-c**). (S)-Reticuline was also clearly detected in the supernatant of strain ABC (**Fig. 4d,e** and **Supplementary Fig. 22d-f**). The (S)-reticuline-producing strain had no detectable (S)-norcoclaurine in the supernatant, indicating that the conversion efficiency from (S)-norcoclaurine to (S)-reticuline was high. To quantify titers, we performed a 96-h fermentation in shake flasks for strains AB and ABC (**Supplementary Fig. 23**). Maximum titers for (S)-norcoclaurine and (S)-reticuline were 104.6 $\mu\text{g l}^{-1}$ and 80.6 $\mu\text{g l}^{-1}$, respectively, and did not show substantial increases after cell saturation. Intracellular product levels were also measured using extraction with methanol. Less than 3% of total (S)-norcoclaurine and (S)-reticuline was observed

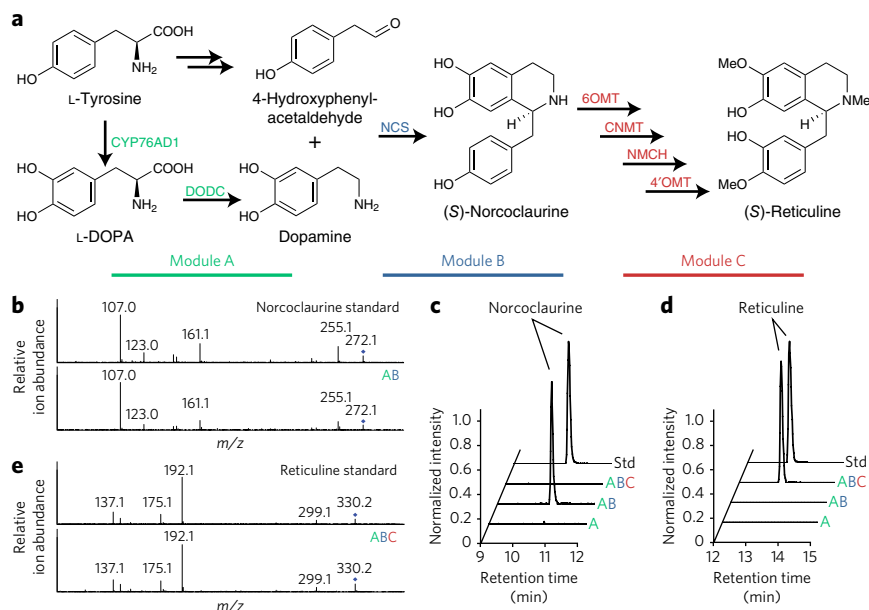


Figure 4 | Production of (S)-reticuline from glucose. (a) The (S)-reticuline pathway was divided into three modules to facilitate analysis. Because 4-HPAA is produced endogenously in *S. cerevisiae* (unlabeled arrows), enzymes catalyzing 4-HPAA synthesis from L-tyrosine were not heterologously expressed. CYP76AD1, tyrosine hydroxylase (W13L F309L double mutant). See **Supplementary Figure 20** for a more detailed pathway diagram of module C. (c,d) LC/MS analysis of norcoclaurine (c) and reticuline (d) in the supernatant of strains expressing modules A, AB and ABC after 48 h of growth in synthetic medium with 4% glucose. Strain AB is engineered to produce norcoclaurine, and strain ABC is engineered to produce reticuline. Traces are normalized to the maximum peak height across all three samples. 'Std' denotes a 5- μ M chemical standard, which was normalized separately. (b,e) MS/MS of norcoclaurine from strain AB (b) and reticuline from strain ABC (e) confirm their identity in comparison to chemical standards. Parent ions are marked with a filled diamond.

in the cell pellet, indicating that these products readily escape into the medium.

Thus, by combining our engineered tyrosine hydroxylase with a newly identified NCS, we demonstrated biosynthesis of the major BIA branch point (S)-reticuline in the industrial workhorse *S. cerevisiae*. This advance establishes a microbial platform in which all BIAs can be synthesized, accelerating the discovery of new enzymes and pathways and the commercial deployment of this technology for industrial-scale production.

DISCUSSION

Microbial production of plant-derived therapeutics promises to transform both pharmaceutical manufacturing and discovery. BIAs are an attractive engineering target given their widespread use and potential to exhibit new pharmacological properties. The length and complexity of the BIA pathway also presents a formidable metabolic engineering challenge that is likely to spur the development of new tools and techniques for controlling the metabolism of microorganisms¹⁶. We report a major breakthrough in microbial BIA production: the development of a yeast strain synthesizing the key intermediate (S)-reticuline from glucose. Although initial titers are low (80.6 μ g/l), this first generation strain marks a starting point for future optimization, which we expect to eventually lead to an alternative, cost-effective method for producing high-value BIAs, thereby dispensing of the need for large-scale dedicated crop cultivation.

(S)-Reticuline production from central metabolites was enabled by a new strategy for intracellular monitoring of L-DOPA that used a plant enzyme to convert L-DOPA into a highly fluorescent small molecule, betaxanthin, that is easy to detect. This tool helped us identify

a previously unknown activity in a cytochrome P450 from beets (CYP76AD1) that filled a longstanding gap in early BIA biosynthesis in yeast. Although wild-type CYP76AD1 had a second activity (DOPA oxidase) that introduces an undesirable side pathway to melanin, we used our L-DOPA biosensor to identify a point mutation that suppresses DOPA oxidase activity and increases flux toward (S)-reticuline.

Although we used the betaxanthin pathway as an enzyme-coupled L-DOPA biosensor to optimize tyrosine hydroxylase activity, we believe that this pathway could prove more generally useful. Because of its fluorescent, water-soluble product, the betaxanthin pathway could be a valuable tool for studying subcellular enzyme localization and metabolite transport or as a model pathway for the development of new high-throughput screening techniques that are amenable to FACS. By linking betaxanthin fluorescence to the production of other metabolites of interest (for example, L-tyrosine), it might be possible to develop high-throughput screens for additional molecules. This work is an example of the rapid progress that is enabled by robust metabolite biosensors.

Further optimization of (S)-reticuline titer will be required before production of downstream BIAs is feasible. Although we achieved a dopamine titer of 23.8 mg l⁻¹, we observed 228-fold lower production of (S)-norcoclaurine (104.6 μ g l⁻¹). It is likely that yeast's endogenous enzymes are largely to blame for inefficiencies at this step. More than 20 potential Ehrlich pathway enzymes could be contributing to the breakdown of 4-HPAA into the side products tyrosol and 4-HPA⁴³. Additionally, the majority of dopamine produced by our strain was found in the supernatant, suggesting that this intermediate is secreted by a yet-to-be-identified transporter. Finally, carefully balancing the production of dopamine and 4-HPAA, both of which are derived from L-tyrosine, may lead to increased yields of (S)-norcoclaurine. Addressing these and other endogenous factors that limit flux will be important for future strain optimization.

Here we have described a foundational advance in microbial BIA synthesis by linking production of the key intermediate (S)-reticuline to yeast central metabolism. As metabolic engineering and synthetic biology tools continue to improve, progress toward a strain capable of high-yielding BIA fermentation from readily available feedstocks will accelerate. Because of the potential for illicit use of these products, including morphine and its derivatives, it is critical that appropriate policies for controlling such strains be established so that we can garner the considerable benefits while minimizing the potential for abuse.

Note added in proof: During the revision of this manuscript, Fossati et al.⁴⁴ described the synthesis of codeine from (R)-reticuline in *S. cerevisiae*.

Received 11 March 2015; accepted 9 April 2015; published online 18 May 2015

METHODS

Methods and any associated references are available in the [online version of the paper](#).

Accession codes. GenBank. The accession code for the DNA sequence for *Papaver somniferum* NCS (PsNCS) is [KP262411](#). The accession codes for all plasmid sequences are listed in **Supplementary Tables 1 and 2**.

References

- Leonard, E., Rungtuphan, W., O'Connor, S. & Prather, K.J. Opportunities in metabolic engineering to facilitate scalable alkaloid production. *Nat. Chem. Biol.* **5**, 292–300 (2009).
- Koehn, F.E. & Carter, G.T. The evolving role of natural products in drug discovery. *Nat. Rev. Drug Discov.* **4**, 206–220 (2005).
- Glenn, W.S., Rungtuphan, W. & O'Connor, S.E. Recent progress in the metabolic engineering of alkaloids in plant systems. *Curr. Opin. Biotechnol.* **24**, 354–365 (2013).
- Paterson, I. & Anderson, E.A. Chemistry. The renaissance of natural products as drug candidates. *Science* **310**, 451–453 (2005).
- Mora-Pale, M., Sanchez-Rodriguez, S.P., Linhardt, R.J., Dordick, J.S. & Koffas, M.A.G. Biochemical strategies for enhancing the *in vivo* production of natural products with pharmaceutical potential. *Curr. Opin. Biotechnol.* **25**, 86–94 (2014).
- Facchini, P.J. *et al.* Synthetic biosystems for the production of high-value plant metabolites. *Trends Biotechnol.* **30**, 127–131 (2012).
- Arkin, A.P. & Fletcher, D.A. Fast, cheap and somewhat in control. *Genome Biol.* **7**, 114 (2006).
- Siddiqui, M.S., Thodey, K., Trenchard, I. & Smolke, C.D. Advancing secondary metabolite biosynthesis in yeast with synthetic biology tools. *FEMS Yeast Res.* **12**, 144–170 (2012).
- Paddon, C.J. *et al.* High-level semi-synthetic production of the potent antimalarial artemisinin. *Nature* **496**, 528–532 (2013).
- Hagel, J.M. & Facchini, P.J. Benzylisoquinoline alkaloid metabolism: a century of discovery and a brave new world. *Plant Cell Physiol.* **54**, 647–672 (2013).
- Beaudoin, G.A.W. & Facchini, P.J. Benzylisoquinoline alkaloid biosynthesis in opium poppy. *Planta* **240**, 19–32 (2014).
- Nakagawa, A. *et al.* A bacterial platform for fermentative production of plant alkaloids. *Nat. Commun.* **2**, 326 (2011).
- Nakagawa, A. *et al.* (R,S)-Tetrahydropapaveroline production by stepwise fermentation using engineered *Escherichia coli*. *Sci. Rep.* **4**, 6695 (2014).
- Hawkins, K.M. & Smolke, C.D. Production of benzylisoquinoline alkaloids in *Saccharomyces cerevisiae*. *Nat. Chem. Biol.* **4**, 564–573 (2008).
- Fossati, E. *et al.* Reconstitution of a 10-gene pathway for synthesis of the plant alkaloid dihydrosanguinarine in *Saccharomyces cerevisiae*. *Nat. Commun.* **5**, 3283 (2014).
- Thodey, K., Galanie, S. & Smolke, C.D. A microbial biomanufacturing platform for natural and semisynthetic opioids. *Nat. Chem. Biol.* **10**, 837–844 (2014).
- Minami, H. *et al.* Microbial production of plant benzylisoquinoline alkaloids. *Proc. Natl. Acad. Sci. USA* **105**, 7393–7398 (2008).
- Mee, M.T., Collins, J.J., Church, G.M. & Wang, H.H. Syntrophic exchange in synthetic microbial communities. *Proc. Natl. Acad. Sci. USA* **111**, E2149–E2156 (2014).
- Zhou, K., Qiao, K., Edgar, S. & Stephanopoulos, G. Distributing a metabolic pathway among a microbial consortium enhances production of natural products. *Nat. Biotechnol.* **33**, 377–383 (2015).
- Lichman, B.R. *et al.* 'Dopamine-first' mechanism enables rational engineering of norcoclaurine synthase aldehyde activity profile. *FEBS J.* **282**, 1137–1151 (2015).
- Fitzpatrick, P.F. Tetrahydropterin-dependent amino acid hydroxylases. *Annu. Rev. Biochem.* **68**, 355–381 (1999).
- Claus, H. & Decker, H. Bacterial tyrosinases. *Syst. Appl. Microbiol.* **29**, 3–14 (2006).
- Halaoui, S., Asther, M., Sigoillot, J.C., Hamdi, M. & Lomascolo, A. Fungal tyrosinases: new prospects in molecular characteristics, bioengineering and biotechnological applications. *J. Appl. Microbiol.* **100**, 219–232 (2006).
- Gandía-Herrero, F., García-Carmona, F. & Escibano, J. Botany: floral fluorescence effect. *Nature* **437**, 334 (2005).
- Sasaki, N. *et al.* Detection of DOPA 4,5-dioxygenase (DOD) activity using recombinant protein prepared from *Escherichia coli* cells harboring cDNA encoding DOD from *Mirabilis jalapa*. *Plant Cell Physiol.* **50**, 1012–1016 (2009).
- Gandía-Herrero, F. & García-Carmona, F. Biosynthesis of betalains: yellow and violet plant pigments. *Trends Plant Sci.* **18**, 334–343 (2013).
- Gandía-Herrero, F., García-Carmona, F. & Escibano, J. A novel method using high-performance liquid chromatography with fluorescence detection for the determination of betaxanthins. *J. Chromatogr. A* **1078**, 83–89 (2005).
- Zhang, J.H., Chung, T. & Oldenburg, K. A simple statistical parameter for use in evaluation and validation of high throughput screening assays. *J. Biomol. Screen.* **4**, 67–73 (1999).
- Santos, C.N.S. & Stephanopoulos, G. Melanin-based high-throughput screen for L-tyrosine production in *Escherichia coli*. *Appl. Environ. Microbiol.* **74**, 1190–1197 (2008).
- Lezzi, C., Blevé, G., Spagnolo, S., Perrotta, C. & Grieco, F. Production of recombinant *Agaricus bisporus* tyrosinase in *Saccharomyces cerevisiae* cells. *J. Ind. Microbiol. Biotechnol.* **39**, 1875–1880 (2012).
- Hernández-Romero, D., Sanchez-Amat, A. & Solano, F. A tyrosinase with an abnormally high tyrosine hydroxylase/dopa oxidase ratio. *FEBS J.* **273**, 257–270 (2006).
- Hatlestad, G.J. *et al.* The beet R locus encodes a new cytochrome P450 required for red betalain production. *Nat. Genet.* **44**, 816–820 (2012).
- Gandía-Herrero, F. & García-Carmona, F. Characterization of recombinant *Beta vulgaris* 4,5-DOPA-extradiol-dioxygenase active in the biosynthesis of betalains. *Planta* **236**, 91–100 (2012).
- Koyanagi, T. *et al.* Eukaryotic-type aromatic amino acid decarboxylase from the root colonizer *Pseudomonas putida* is highly specific for 3,4-dihydroxyphenyl-L-alanine, an allelochemical in the rhizosphere. *Microbiology* **158**, 2965–2974 (2012).
- Luttik, M.A.H. *et al.* Alleviation of feedback inhibition in *Saccharomyces cerevisiae* aromatic amino acid biosynthesis: quantification of metabolic impact. *Metab. Eng.* **10**, 141–153 (2008).
- Gandía-Herrero, F., Escibano, J. & García-Carmona, F. Characterization of the activity of tyrosinase on betanidin. *J. Agric. Food Chem.* **55**, 1546–1551 (2007).
- Dohm, J.C. *et al.* The genome of the recently domesticated crop plant sugar beet (*Beta vulgaris*). *Nature* **505**, 546–549 (2014).
- Pieper, U. *et al.* ModBase, a database of annotated comparative protein structure models and associated resources. *Nucleic Acids Res.* **42**, D336–D346 (2014).
- Sentheshanmuganathan, S. & Elsdén, S.R. The mechanism of the formation of tyrosol by *Saccharomyces cerevisiae*. *Biochem. J.* **69**, 210–218 (1958).
- Pauli, H.H. & Kutchan, T.M. Molecular cloning and functional heterologous expression of two alleles encoding (S)-N-methylcoclaurine 3'-hydroxylase (CYP80B1), a new methyl jasmonate-inducible cytochrome P-450-dependent mono-oxygenase of benzylisoquinoline alkaloid biosynthesis. *Plant J.* **13**, 793–801 (1998).
- Xiao, M. *et al.* Transcriptome analysis based on next-generation sequencing of non-model plants producing specialized metabolites of biotechnological interest. *J. Biotechnol.* **166**, 122–134 (2013).
- Minami, H., Dubouzet, E., Iwasa, K. & Sato, F. Functional analysis of norcoclaurine synthase in *Coptis japonica*. *J. Biol. Chem.* **282**, 6274–6282 (2007).
- Hazelwood, L.A., Daran, J.-M., van Maris, A.J.A., Pronk, J.T. & Dickinson, J.R. The Ehrlich pathway for fusel alcohol production: a century of research on *Saccharomyces cerevisiae* metabolism. *Appl. Environ. Microbiol.* **74**, 2259–2266 (2008).
- Fossati, E., Narcross, L., Ekins, A., Falgoutyret, J.P. & Martin, V.J.J. Synthesis of morphinan alkaloids in *Saccharomyces cerevisiae*. *PLoS ONE* **10**, e0124459 (2015).

Acknowledgments

We thank H. Lee for assistance with preliminary experiments; S. Bauer for LC/MS training; members of the Martin and Duebber Labs, in particular M. Lee, for valuable feedback throughout the project and in the preparation of the manuscript; and L. Bourgeois and J. Scrivens for their contribution in identifying NCS enzymes active in yeast. The work on engineering an enzyme-coupled biosensor was supported by the US Department of Energy Office of Science Early Career Research Program (Office of Biological and Environmental Research) under award number DE-SC0008084 (grant to J.E.D.), the US National Science Foundation (fellowship to W.C.D.) and the US Department of Defense (fellowship to Z.N.R.). Research in the Martin lab was financially supported by Genome Canada, Genome Québec and a Canada Research Chair (V.J.J.M.).

Author contributions

W.C.D., Z.N.R., L.N., V.J.J.M. and J.E.D. designed the research. W.C.D. and Z.N.R. performed the experiments, and L.N. conducted chiral analysis. A.M.G. assisted in preliminary studies. W.C.D., Z.N.R. and L.N. analyzed the results. V.J.J.M. and J.E.D. supervised the research. W.C.D., V.J.J.M. and J.E.D. wrote the manuscript with editing help from Z.N.R. and L.N.

Competing financial interests

The authors declare competing financial interests: details accompany the [online version of the paper](#).

Additional information

Supplementary information is available in the [online version of the paper](#). Reprints and permissions information is available online at <http://www.nature.com/reprints/index.html>. Correspondence and requests for materials should be addressed to J.E.D.

ONLINE METHODS

Strains and growth media. The base *S. cerevisiae* strain for all experiments in this article was BY4741 (*MATa his3Δ1 leu2Δ0 met15Δ0 ura3Δ0*). Wild-type yeast cultures were grown in YPD (10 g/l Bacto Yeast Extract, 20 g/l Bacto peptone, 20 g/l dextrose). Selection of auxotrophic markers (URA3, LEU2 and/or HIS3) was performed in synthetic complete medium (6.7 g/l Difco Yeast Nitrogen Base without amino acids (Spectrum Chemical), 2 g/l Drop-out Mix Synthetic minus appropriate amino acids without Yeast Nitrogen Base (US Biological), 20 g/l dextrose). All of the strains constructed in this work are listed in **Supplementary Table 1**.

Golden gate assembly reactions were transformed in TG1 chemically competent *E. coli*. Error-prone PCR libraries were transformed in TransforMax EPI300 (Epicentre) electrocompetent *E. coli*. Transformed cells were selected on Lysogeny Broth (LB) containing the antibiotics ampicillin or kanamycin.

Yeast expression vectors. Yeast expression vectors were built using Golden Gate Assembly⁴⁵. Vector sequences were derived from the pRS series of plasmids. Promoter and terminator sequences for heterologous enzyme expression were derived from the yeast genome. Unique restriction sites (BsaI and BsmBI) were removed to facilitate plasmid construction.

Error-prone PCR library plasmids included a CEN6/ARS4 low copy number origin of replication to enable high-efficiency library transformations, as did the expression plasmid for the reticuline pathway enzymes (module C). All other plasmids contained no yeast origin of replication and were designed for direct integration into the yeast genome via homologous recombination at the URA3 or LEU2 locus. All strains and plasmids used in this work have been deposited in GenBank, and the accession codes are listed in **Supplementary Tables 1 and 2**.

Yeast strain construction. Aside from mutant libraries and the reticuline production strain ABC (Strain 33; **Supplementary Table 1**), all of the genetic modifications to yeast were made via genomic integration. Yeast integration plasmids (YIPs) were constructed that lacked a yeast origin of replication but included regions of homology to either the URA3 or LEU2 locus. Five hundred micrograms of plasmid was linearized by digestion with NotI and transformed directly into yeast using a standard lithium acetate transformation. Cells were plated onto dropout plates corresponding to the YIP's auxotrophic marker. Replicate colonies were picked directly from this transformation plate for further analysis.

L-DOPA titrations for betaxanthin production. Strains 1 and 3 were grown overnight in synthetic complete medium (minus uracil) with 2% glucose. Saturated cultures were back-diluted 100× into fresh medium supplemented with L-DOPA (Sigma no. D9628) and grown in 24-well or 96-well blocks with shaking at 30 °C for 24 h. L-DOPA concentrations ranged from 10,000 μM to 0.15 μM in twofold increments. Cells were spun down and washed in PBS (pH 7.4), and betaxanthin was quantified on either a microplate fluorometer or a flow cytometer (see below).

Flow cytometry. A guava easyCyte flow cytometer (EMD Millipore) was used to quantify betaxanthin fluorescence at an excitation of 488 nm and emission of 510 nm with a gain setting of 20. Cells were gated for forward and side scatter as shown in **Supplementary Figure 3**. Betaxanthin fluorescence was normalized to forward scatter to account for differences in cell size. Histograms were prepared, and data analysis was performed using the software package FlowJo (<http://flowjo.com/>).

Fluorescence microscopy. For analysis of intracellular betaxanthin (**Fig. 1b**), Strain 2 was grown with or without 1 mM L-DOPA in synthetic complete medium (minus uracil) with 2% glucose overnight. Cultures were concentrated by centrifugation, washed in PBS (pH 7.4), and spotted onto plain glass slides to be examined with an Observer D1 microscope (Zeiss) using a 100× DIC objective. Images were captured using a Orca-flash 4.0 camera (Hamamatsu no. C11440) using auto-exposure. Fluorescence images were taken using an X-Cite Series 120 lamp (Excelitas) and filter set 45 (Zeiss), with excitation at 560/40 nm and emission at 630/75 nm for mKate2 and filter set 46 (Zeiss) with excitation at 500/20 nm and emission at 535/30 nm for betaxanthin²⁴.

Intracellular CYP76AD1 localization was analyzed via C-terminal fusion of the yellow fluorescent protein Venus to each enzyme variant and visualization on a spinning disk confocal microscope. Strains 41–44 were grown to saturation

in SD-uracil and back-diluted 50× into fresh medium. After 6 h of growth at 30 °C, cells were concentrated by centrifugation, washed in PBS (pH 7.4) and spotted onto plain glass slides to be examined with a CSU-X1 spinning disk confocal microscope (Yokogawa) using a 100× bright-field objective and a 488-nm excitation laser. Images were taken using a QuantEM 512SC EMCCD camera (Photometrics) and analyzed using Fiji (<http://fiji.sc/>).

Error-prone PCR library construction. Error-prone PCR was performed using the GeneMorph II Random Mutagenesis Kit (Agilent Technologies). Oligos 1 and 2 (**Supplementary Table 3**) were used to amplify the CYP76AD1 coding sequence off of the template for PCR (Plasmid 1; **Supplementary Table 2**). Plasmid template was added to the PCR reaction at a concentration of 40 ng/μl to achieve the desired error rate. The PCR reaction was run as suggested in the GeneMorph II user manual, using an annealing temperature of 45 °C.

The PCR was incubated with DpnI for 1 h at 37 °C before being cleaned up using a DNA Clean and Concentrator kit (Zymo Research). A BsaI Golden Gate Assembly reaction was run using 40 fmol of both the PCR product and Plasmid 2. This reaction was again cleaned up, eluted in 10 μl of water and transformed in its entirety into TransforMax EPI300 (Epicentre) electrocompetent cells. After a 1-h rescue, the cells were grown to saturation in 500 ml of LB plus kanamycin overnight. Two milliliters of saturated culture was mini-prepped, and all resulting DNA was transformed into Strain 3 for screening using a standard LiOAc transformation.

DNA shuffling library construction. CYP76AD1 mutants were shuffled using Golden Gate Shuffling⁴⁶. The coding sequence was divided into four regions that equally distributed the set of mutations being shuffled. Oligos 5–14 were used to PCR amplify fragments using the mutant plasmids as templates. These PCRs were mixed in a Golden Gate Assembly reaction and prepped for library screening as described in the above section on error-prone PCR library construction.

Library screening for improved betaxanthin production. For screening of tyrosine hydroxylase mutants, yeast transformations were plated on multiple 500-cm² agar plates (with synthetic dropout medium) at a density of approximately 50,000 colonies per plate. After 72 h of growth at 30 °C, the most intensely yellow colonies were isolated for further analysis. To aid in the selection of high-producing colonies, 470 nm blue LED light epi-illumination was applied to the plates and viewed through an amber high-pass emission filter.

Betaxanthin fluorescence quantification. Colonies were picked into synthetic complete media with 2% glucose and grown overnight. Saturated cultures were back-diluted 50× into fresh media in 96-deep-well blocks. Cultures were grown for 48 h in a Multitron shaker (Appropriate Technical Resources) at 30 °C. Cells were pelleted, washed and resuspended in PBS (pH 7.4). The cells were transferred to glass-bottomed microplates and measured for fluorescence in a Safire2 microplate reader (TECAN) (excitation: 485/5 nm, emission: 505/5 nm, gain: 120) (ref. 24). Fold change over background fluorescence measurements was calculated by normalizing to the average fluorescence observed in control Strain 4.

Production assay for L-DOPA, dopamine, dopaquinone and melanin. Colonies were picked into 2.5 ml of 2× synthetic complete medium (minus uracil) with 4% glucose. After overnight growth, saturated cultures were back-diluted 50× into 24-deep-well blocks with fresh medium. The cultures were grown in a Multitron shaker (Appropriate Technical Resources) for 48 h at 30 °C. Cultures were pelleted, and culture supernatants were measured for titer via LC/MS in the case of L-DOPA, dopamine and dopaquinone. For dopaquinone production, 10 mM ascorbic acid was added to the growth medium to prevent oxidation of this unstable product. In the case of melanin production, pellets were photographed directly.

Western blotting. Strains 1 and 22–25 were grown to saturation in synthetic complete medium (minus uracil) with 2% glucose overnight and back-diluted 50× into fresh medium. After 6 h of growth with shaking at 30 °C, cells at 2.5 OD were pelleted, washed in water, resuspended in 200 mM NaOH and incubated at room temperature for 5 min. Cells were again pelleted, resuspended in 50 μl of PAGE sample buffer and boiled at 95 °C for 5 min. Samples were diluted tenfold in PAGE sample buffer, and 8 μl was loaded onto a NuPAGE Novex 4–12% Bis-Tris gel (Life Technologies) and run for 2.5 h at 80 V.

Proteins were transferred onto PVDF transfer membrane in NuPAGE transfer buffer (Life Technologies) and blocked overnight in TBST (0.05% Tween20) with 5% milk. The membrane was washed twice with TBST for 5 min and incubated for 1 h with HRP conjugated anti-Flag (Sigma no. A8592) and anti-GAPDH (Fisher Scientific no. MA515738HRP) monoclonal antibodies at dilutions of 1:5,000 and 1:10,000, respectively. After six 5-min washes in TBST, the HRP antibodies were detected by chemiluminescence using a ChemiDoc XRS imager (Bio-Rad), and the blots was analyzed using Fiji (<http://fiji.sc/>).

Expression level quantification via fluorescent protein fusion. Colonies of Strains 1 and 41–44 were grown in 96-deep-well blocks in synthetic complete media minus uracil to saturation and back-diluted into fresh medium. After 24 h of growth with shaking at 30 °C, 100 µl of each culture was transferred to a glass-bottomed microplate and measured for fluorescence in a Safire2 microplate reader (TECAN; excitation 516/5nm, emission 530/5nm, gain 100). Fold changes over background measurements were obtained by normalizing all fluorescence values to the average fluorescence observed in control Strain 1.

Betalain production assay. Special medium was required to observe the production of betanidin in culture supernatants. We discovered that the standard medium component *para*-aminobenzoic acid (PABA) was capable of spontaneous condensation with betalamic acid to produce PABA-betaxanthin. PABA-betaxanthin had similar absorbance properties to betanidin, making it difficult to visualize changes in betanidin formation.

We therefore prepared minimal medium lacking PABA (7.6 g/l Yeast Nitrogen Base without amino acids or vitamins (Difco), 76 mg/l histidine, 76 mg/l methionine, 76 mg/l tryptophan, 380 mg/l leucine, 2 mg/l biotin, 400 mg/l calcium pantothenate, 2 g/l inositol, 400 mg/l pyridoxin HCL, 400 mg/l thiamine HCL, 20 g/l dextrose).

Cells were first grown to saturation in synthetic complete medium (minus uracil) with 2% glucose. They were then back-diluted 50× into our custom minimal medium, which was supplemented with 10 mM ascorbic acid to prevent betanidin oxidation and 1 mM tyrosine. Cultures were grown in 24-deep-well blocks at 30 °C in a Multitron shaker (Appropriate Technical Resources) for 24 h. Cells were pelleted, and supernatants were analyzed. Absorbance spectra of culture supernatants were acquired using a Safire2 microplate reader (TECAN). LC/MS analysis was performed as described below.

Shake-flask fermentations for norcoclaurine and reticuline. Colonies were picked into 2.5 ml of selective synthetic medium with 2% glucose. After overnight growth, saturated cultures were back-diluted 50× into 250 ml baffled shake flasks containing 50 ml of fresh 2× selective synthetic medium with 4% glucose. The cultures were grown at 30 °C with shaking at 220 r.p.m. for 96 h in an Innova 44 incubator (Eppendorf). At designated time points, aliquots were taken from the cultures to measure OD₆₀₀, and the medium was stored at –20 °C for later analysis by LC/MS.

LC/MS analysis. Pellet extraction using acetonitrile. One milliliter of each cell culture was centrifuged at 3,000 RCF for 5 min to collect cells. The cells were then washed with 1 ml of PBS (pH 7.4), centrifuged again and resuspended in 500 µl of PBS containing 35 U of zymolyase (Zymo Research). This was then incubated at 37 °C for 1 h to spheroplast the yeast. After incubation, 500 µl of acetonitrile was added to disrupt cells and precipitate protein. The mixture was vortexed for 1 min and centrifuged at 14,000 RCF to remove precipitate. Finally, the supernatant was concentrated under vacuum to one-tenth its original volume.

HPLC absorbance traces. Ten microliters of each culture supernatant or extract was separated on a 1260 Infinity Quaternary LC System (Agilent Technologies) with a Zorbax Eclipse Plus C18 4.6 × 100 mm-3.5 µm reversed-phase column (Agilent Technologies) at ~20 °C using a 0.5 ml/min flow rate. Samples were eluted with a linear gradient from 100% water/0% acetonitrile plus 0.1% formic acid to 65% water/35% acetonitrile plus 0.1% formic acid over the course of 15 min. Absorbance was measured using a diode array detector at 405 nm (betalamic acid), 480 nm (betaxanthin) and 536 nm (betanidin) with 4-nm bandwidth. MS was carried out using an attached 6120 Quadrupole LC/MS (Agilent Technologies) in atmospheric pressure ionization–positive electrospray (API-ES positive) mode at 100-V fragmentor voltage, scanning masses between 100 Da and 700 Da. Peak identification was additionally assisted by ion extraction of betalamic acid (m/z 212.055 and R_t 11.0 min), tyrosine-betaxanthin/portulacaxanthin II (m/z 375.119 and R_t 10.9 min),

betanidin (m/z 389.098 and R_t 10.3 min) as well as proline-betaxanthin (m/z 309.110 and R_t 8.8 min), valine-betaxanthin (m/z 311.125 and R_t 11.3 min), (iso)leucine-betaxanthin (m/z 325.139 and R_t 13.1 or 13.4 min), phenylalanine-betaxanthin (m/z 359.123 and R_t 13.7 min) and tryptophan-betaxanthin (m/z 398.1357 and R_t 14.5 min). Traces were collected and analyzed using ChemStation (Agilent Technologies).

LC/MS quantification of L-DOPA and derivatives-DOPA and derivatives. Quantitative MS and MS/MS data were collected with the same column, pump and gradient as above but using a 6520 Accurate-Mass Q-TOF LC/MS (Agilent Technologies) for fragmentation and mass detection. The system was run in positive electrospray (ESI+) mode with a 100-V fragmentor voltage and, for MS/MS, a collision energy of 23 V. For quantification of betalamic acid (m/z 212.055 and R_t 11.0 min), tyrosine-betaxanthin/portulacaxanthin II (m/z 375.119 and R_t 10.9 min) and betanidin (m/z 389.098 and R_t 10.3 min), extracted ion counts were integrated and normalized against eight-point relative standard curves generated by repeated twofold dilutions of threefold concentrated supernatant from Strain 8 (betanidin) or Strain 9 (tyrosine-betaxanthin). Dopamine was quantified by ion extraction at m/z 196.06 and R_t 2.8 min; peaks were integrated and reported. For quantification of dopamine, ion counts with m/z of 154.086 [M+H]⁺ and a retention time of 3.0 min were extracted, integrated and quantified against an eight-point dopamine calibration curve ranging from 0.004 mM to 1 mM in twofold steps. Other species targeted were norcoclaurine (m/z 272.121 [M+H]⁺ and R_t 10.7 min) and reticuline (m/z 330.17 [M+H]⁺ and R_t 13.3 min). For quantification purposes, these extracted ion counts were integrated and compared against six-point calibration curves covering 0.078–2.50 µM and 0.039–1.25 µM in twofold steps for norcoclaurine and reticuline, respectively. These calibration curves were generated using (S)-norcoclaurine and (R)-reticuline authentic standards (Toronto Research Chemicals Inc.). Traces were analyzed, extracted and quantified using MassHunter (Agilent Technologies) and MzMine2 (<http://mzmine.sourceforge.net/>).

Norcoclaurine chiral analysis. Culture supernatant from Strain 32 was concentrated 10× by SpeedVac, resuspended 1:2 in MeOH and centrifuged at 21,000g for 30 s. Norcoclaurine enantiomers were analyzed by reverse-phase HPLC using a Series 200 Micropump (PerkinElmer) equipped with a Shodex ORpak CDBS-453 column (FUJEC Chromatography). Ten microliters of supernatant was loaded on the column and separated using the following gradient: 0–35 min 5% B, 35–38 min 95% B, 38–45 min 5% B at a flow rate of 250 µl/min, where Solvent A was 0.1% acetic acid and Solvent B was 80:20:1 acetonitrile/methanol/acetic acid. Following separation, eluent was injected into a 7T-LTQ FT ICR instrument (Thermo Scientific). Norcoclaurine was identified by exact mass (m/z 272.128 [M+H]⁺). Spontaneously condensed (R,S)-norcoclaurine, generated through resuspension of an equal ratio of L-dopamine (Sigma) and 4-HPAA (gift from P. Facchini, University of Calgary) in H₂O, and (S)-norcoclaurine standard (Toronto Research Chemicals Inc.) were used to determine retention time of each enantiomer. Curves were smoothed with a seven-point boxcar average.

Reticuline chiral analysis. Determination of reticuline enantiomers in Strain 33 supernatant was performed by HPLC-FT-MS. Yeast supernatant was concentrated 200× using a SepPak Light C18 cartridge (Waters Corporation) and then resuspended 1:7 in MeOH and centrifuged at 21,000g for 30 s. Reticuline enantiomers were analyzed by standard-phase HPLC using a Series 200 Micropump (PerkinElmer) equipped with a 4.6 × 250 mm CHIRALCEL OD-H column (Daicel Chemical Industries) heated to 40 °C. Five microliters of supernatant was loaded on the column and separated using an isocratic mixture of 72:28:0.001 hexane/isopropanol/diethylamine at a flow rate of 0.55 ml/min¹². Following separation, eluent was injected into a 7T-LTQ FT ICR instrument (Thermo Scientific). Reticuline was identified by exact ion mass (m/z 330.17 [M+H]⁺). Authentic (R)-reticuline (Toronto Research Chemicals Inc.) and (S)-reticuline (gift from P. Facchini, University of Calgary) were used as standards to determine retention time of each enantiomer. Curves were smoothed with a seven-point boxcar average.

45. Weber, E., Engler, C., Gruetzner, R., Werner, S. & Marillonnet, S. A modular cloning system for standardized assembly of multigene constructs. *PLoS ONE* 6, e16765 (2011).
46. Engler, C., Gruetzner, R., Kandzia, R. & Marillonnet, S. Golden gate shuffling: a one-pot DNA shuffling method based on type IIs restriction enzymes. *PLoS ONE* 4, e5553 (2009).